Journal of
Manufacturing and Materials Processing

MDPI

Article

Optimization of Surface Roughness of Aluminium RSA 443 in Diamond Tool Turning †

Gregoire Mbangu Tambwe [1,2,*] and Dirk Pons [2,*]

[1] Department of Mechatronics Engineering, Faculty of Engineering and Built Environment, Nelson Mandela University, Port Elizabeth 6031, Eastern Cape, South Africa
[2] Department of Mechanical Engineering, University of Canterbury, Christchurch 8041, New Zealand
* Correspondence: gregory.mbangu@pg.canterbury.ac.nz or gregorymbangu@yahoo.com (G.M.T.); dirk.pons@canterbury.ac.nz (D.P.)
† Publication declaration: This paper is a derivative work of the following thesis: Gregoire, M.T., Optimization of surface roughness of alumimium grade (RSA 443) in diamond tool turning. Nelson Mandela University, 2021. Master of Engineering thesis.

Abstract: Context—Rapidly solidified aluminium alloy (RSA 443) is increasingly used in the manufacturing of optical mold inserts because of its fine nanostructure, relatively low cost, excellent thermal properties, and high hardness. However, RSA 443 is challenging for single-point diamond machining because the high silicon content mitigates against good surface finishes. Objectives—The objectives were to investigate multiple different ways to optimize the process parameters for optimal surface roughness on diamond-turned aluminium alloy RSA 443. The response surface equation was used as input to three different artificial intelligence tools, namely genetic algorithm (GA), particle swarm optimization (PSO), and differential evolution (DE), which were then compared. Results—The surface roughness machinability of RSA443 in single-point diamond turning was primarily determined by cutting speed, and secondly, cutting feed rate, with cutting depth being less important. The optimal conditions for the best surface finish Ra = 14.02 nm were found to be at the maximum rotational speed of 3000 rpm, cutting feed rate of 4.84 mm/min, and depth of cut of 14.52 µm with optimizing error of 3.2%. Regarding optimization techniques, the genetic algorithm performed best, then differential evolution, and finally particle swarm optimization. Originality—The study determines optimal diamond machining parameters for RSA 443, and identifies the superiority of GA above PSO and DE as optimization methods. The principles have the potential to be applied to other materials (e.g. in the RSA family) and machining processes (e.g. turning, milling).

Keywords: response surface methodology; precision machining; diamond turning

Citation: Mbangu Tambwe, G.; Pons, D. Optimization of Surface Roughness of Aluminium RSA 443 in Diamond Tool Turning. *J. Manuf. Mater. Process.* **2024**, *8*, 61. https://doi.org/10.3390/jmmp8020061

Academic Editor: Steven Y. Liang

Received: 16 February 2024
Revised: 4 March 2024
Accepted: 8 March 2024
Published: 19 March 2024

1. Introduction

During the last three decades of the 1900s, ultra-precision machining techniques have successfully been applied to machine precise parts, for example, lens, computer memory discs for hard drives, and photoreceptors for photocopier machines. These applications demand highest surface accuracies. Single-point diamond turning had been effectivity used to machine these surfaces, in contrast to multi processes such as lapping and polishing [1]. The focus of the current work is on single-point diamond turning.

The manufacturing of molded optical components uses materials such as steel, aluminium, and tungsten carbide for the molds. Heat resistance, reflective properties, and characteristic strength are key selection criteria [2]. Rapidly solidified aluminium alloy (RSA 443) is increasingly used in the manufacturing of optical mold inserts because of its fine nanostructure, relatively low cost, excellent thermal properties, and high hardness. However, RSA 443 is challenging for diamond machining because the high silicon content

mitigates against good surface finishes. Control of surface roughness in the manufacturing process is important for production quality [3]. Typical process parameters for diamond are cutting speed, cutting feed rate, and cutting depth [4], and these affect the surface roughness. However, optimizing these parameters for surface quality is not straightforward and is dependent on the material grade [5]. This paper describes a method to determine the optimal process parameters using statistical methods and artificial intelligence (AI), for RSA 443, based on [6]. The method uses the response surface methodology followed by a variety of processes of which genetic algorithms are shown to be the best.

2. Literature on Diamond Machining Generally and RSA Specifically

2.1. Diamond Turning

Diamond machining has also been used to create fine structures such as microcavities [7] and sinusoidal gratings [8]. Ultra-precision manufacturing approach is applied to the optics production on a range of conventional engineering materials in single-point diamond turning (SPDT) [9]. Examples include astronomy optics [10]. Furthermore, SPDT operation produces the parts with a much better metallurgic structure than through polishing and lapping procedures [11].

2.1.1. Tool Wear

In the case of ferrous materials, diamond tools can wear via a reaction with the substrate that causes the diamond to graphitize. Wear may be partly suppressed by the application of magnetic fields [12]. Investigation has been carried out for the influence of different machining factors on the diamond tool-tip wear during the SPDT of optical grade silicon; thus, the selection and control of cutting parameters must finely controlled [13]. To establish a theoretical prediction model to find the optimized cutting parameters for the minimum surface roughness is an objective of SPDT operations.

2.1.2. Tool Path Considerations

Regarding tool path considerations for diamond turning, the key consideration is surface topography [14]. This requires cutting testing optimization [15] or other systematic methods to generate the appropriate tool path [16]. Slow tool servo (STS) approaches have been used to generate nanometric surface topography [17].

2.1.3. Hybrid Methods

Hybrid methods, or non-conventional machining, involves removal of processing disturbances by means of automatic metrology and control systems [18] or ultrasonic vibration control [19] to produce higher quality of optical surfaces [20]. Dynamic systems attempt to remove processing disturbances during mechanical contacts between the tool and workpiece [20]. However, these methods require sensors [21], which may include interferometry systems, and hence, more complex production setups. In addition, the material removal process becomes more complex by the addition of further process settings and control loops, and hence, optimization becomes more challenging.

2.2. Machining of RSA Materials

There is intensive application of ultra-high precision machining to the photonic industry to produce optical surfaces. A common material is aluminium, and in these applications, there is demand for optical aluminium material with consistent properties [22]. A typical alloy to create optical surfaces is AA 6061 [23]. In this area, RSA alloys have been shown to be effective and cost effective [24]. The benefits of RSA arise from their finer microstructures and improved mechanical and physical properties [25]. RSA 905 is the modification of aluminium grade of 6061 and has a finer microstructure due to the rapid solidification melting process, and has been used successfully [26]. Another one of these

alloys is RSA 443 (40% of silicon and 60% aluminium) which likewise has a fine nanostructure [27]. However the anisotropic nature of RSA materials is a challenge because it affects surface roughness in ways that are difficult to predict [21]. To some extent, this is being addressed by molecular dynamic simulations [28]; however, this technique is limited to small ensembles of atoms, often in a single plane, which is not truly representative of three-dimensional geometry.

Diamond tooling has been shown to be effective for machining RSA 905, with tool wear being low [29]. For RSA 443, the highest tool wear has been observed at a greater depth of the cut and feed rate [30]. The minimum quantity lubrication (MQL) method has been shown to reduce the consumption of cutting fluids volume [31]. MQL can be applied to reduce adhesion wear, and thus improve surface roughness.

The surface quality of diamond machined RSA alloys has also been approached from the theory of chip flow (using finite elements), and the results showed dependency on process parameters, with an underlying mechanism being subsurface damage from the removal of precipitate particles [32]. Optimal process parameters for RSA 905 have been identified as having a cutting speed of 1750 rpm, a feed rate of 5 mm/min, a depth of cut of 25 μm, and a surface roughness R_a of 3.2 nm [5]. By comparison, process parameters for the diamond turning of polycarbonate have been identified to be 800–4000 rpm, 0.5–4 μm/rev, a depth of 2 μm [33], and for aluminium alloy 6061, reported values are 500–3000 rpm, 5–25 mm/min, a depth of 2–20 μm [34], and for micro grooving of copper, 6–300 rpm, and for feed dependent on thread pitch, a depth of 1–18 μm [35].

2.3. Optimization of Turning Parameters

Finding an optimization between the turning parameters (cutting speed, cutting feed rate, and cutting depth) is not straight forward. Generally, small depths of cut result in better surface roughness [21]. However, this results in longer machining times, thus, adversely affecting production economics. Hence, there is value in optimizing the process parameters.

Several methods have been applied in the literature. Cutting parameters optimization always uses a theoretical predictive model to find the smallest surface roughness in SPDT operations [36]. The response surface methodology (RSM) [37,38] is a general method for finding an optimization across multiple parameters. Box–Behnken Design (BBD) is one of the more popular methods. There have been numerous studies to investigate the application of RSM. For instance, [39] developed a surface roughness model for turning high-strength low-alloy steel (AISI 4340). A recent study by [40] concluded that variance analysis (ANOVA) could be applied to determine the critical states of cutting parameters while RSM optimizes cutting parameters. Further, RSM has been used to establish a surface roughness prediction model for stainless steel [41], and the machinability (material removal rate, tool wear rate, and roughness) of TiB2 reinforcement in AA6061 composites with Electrical Discharge Machining [42]. Additionally, surface vibration data (from 316 stainless steel) have been used to predict surface roughness using an artificial neural network [43].

Another optimization approach is provided by genetic algorithm (GA). It optimizes by an evolutional competitive process, analogous to biological genetic evolution [44] but using computation algorithms [45]. With application of GA in manufacturing, the cutting parameters are considered as genes to be selected according to their fitness. Fitness in this context refers to surface roughness. Previous works include optimizing the surface roughness of mild steel [46] and glass fibre reinforced plastic composite [47], and carbon fibre reinforced plastic [48]. Regarding application to diamond turning, the literature is sparse. One study using a polycrystalline diamond tool used GA (specifically, non-dominated sorting genetic algorithm II) to optimize tool wear and surface roughness, but found the solutions could not be differentiated from each other [49]. For single diamond tools, GA has been applied to the optimization of surface roughness for aluminium substrates [50].

Particle swarm optimization (PSO) is a searching algorithm which uses the simulation of bird movement in a flock. For manufacturing, the birds (or particles) are the cutting parameters, and they are assumed to affect each other locally (neighbour's positioning) and globally. The PSO method has been applied to optimize the surface roughness for a variety of materials and processes, e.g. hard turning (without lubricant) [51], milling [52], turning of steel [53], self-propelled rotary tool turning of steel [54], polymer composites [55], and microchannel manufacture [56]. The literature has many examples of PSO applied to conventional metal removal processes; however, the only extant literature on single-point diamond turning using PSO appears to be [36].

Differential evolution (DE) is another AI technique which uses a strategy of search based on the population. It additionally consists of chromosomes that are evaluated by a fitness function. DE differs from GA in terms of its selection, reproduction, and mutation operators. In DE, mutation is first applied to a parent chromosome to produce a testing vector that is utilized in a crossover with this parent to create offspring. The step sizes of mutation are affected by the difference into two separated individuals of the present population [57]. If the offspring is fitter than the parent, it will be carried over to the next generation; otherwise, the parent will be carried over. As a result, the fitness of the population improves over time. Computationally, this method has been shown to be superior to others [58]. No manufacturing publications exist for DE; nonetheless, other applications exist such as the optimization of photovoltaic models under diverse conditions and environments [59].

In general, the literature shows that optimizing the process parameters for surface quality is difficult to do. The parameters are also dependent on the material grade. A variety of methods exist, including AI. However, there is a need to evaluate the relative effectiveness of the available methods, including DE, which has not previously been applied to this type of area. The material under examination is RSA 443, for which research into process parameters is scarce.

3. Materials and Methods

3.1. Research Objectives

The objectives were to investigate multiple different ways to optimize the process parameters for optimal surface roughness on diamond-turned aluminium alloy RSA 443. The response surface equation was used as input to three different AI tools, namely GA, PSO, and DE, which were then compared.

3.2. Approach

The overall approach was as follows. First, machining data were obtained for a variety of independent variables, with the corresponding surface roughness. Then, the response surface was determined. This provided the necessary fitness function needed for the last part, which was the application of a variety of artificial intelligence methods. These steps are elaborated below.

3.2.1. Experimental Design and Data Collection

Three machining parameters were selected for testing: the cutting parameters were cutting speed (s) (500–3000 rpm), cutting feed rate (f) (5–25 mm/min), and cutting depth (d) (5–25 μm). The experimental space was designed using a Box–Behnken design ('Design Expert' software version 5).

The surface roughness data for RSA 443 were experimentally determined by others in the research group, reported in [60] and given in Table 1 below. They reported that specimens were cut from an RSA 443 round bar, machined on a Nanoform 250 Precision Lathe (Ametek Precitech Inc., Keene, NH, USA), and measured for surface roughness Ra (nm) using a Form Taylor PGI Optics (3D) profilometer (Taylor Hobson Ltd., Leicester, UK). The diamond tool insert (Contour Fine Tool BV, Valkenswaard, The Netherlands.)

had a nose radius of 0.5 mm, rake angle of −5° (mounted on a 0° tool holder), front clearance of 10 ° (mounted on a 0° tool holder), and a standard waviness.

Table 1. Box–Behnken and surface roughness experimental results.

Run	Cutting Speed (s) (rpm)	Cutting Feed Rate (f) (mm/min)	Cutting Depth (d) (μm)	Surface Roughness Ra (nm)
1	1750	25	25	39.33
2	1750	25	5	35.55
3	3000	5	15	14.48
4	1750	15	15	23.94
5	1750	15	15	24.0
6	1750	5	25	17.45
7	500	15	25	76.82
8	3000	25	15	26.22
9	3000	15	25	22.05
10	500	15	15	187.18
11	3000	15	5	26.20
12	500	5	15	28.42
13	1750	5	5	17.35
14	1750	15	15	23.8
15	500	15	5	66.81

3.2.2. Response Surface Methodology Model

The response surface methodology (RSM) approach is the procedure to determine the relation between cutting parameters with various machining criteria. In the work, RSM was also used to determine the relationship between the input cutting parameters with the surface roughness. A second order polynomial response surface mathematical model was developed, and given by following equation:

$$y = \beta_0 + \sum_{i=1}^{3} \beta_i x_i + \sum_{i=1}^{3} \beta_{ii} x_i^2 + \sum_{i} \sum_{j=1} \beta_{ij} x_i x_j + \varepsilon \quad (1)$$

The dependent variable, y, is the response and the independent variable, x is the factor. β are the coefficients estimated from RSM analysis. After determining the significant coefficients (at 95% confidence level), the final model was developed using these coefficients and the final mathematical model to estimate surface roughness is given in Equation (1).

3.2.3. Optimization Techniques

The next objective was to determine the optimal process parameters for minimum surface roughness. The response surface equation was used as input to three different AI tools, namely GA, PSO, and DE, to determine optimal process parameters. MATLAB was used to run the GA, PSO, and DE optimization.

3.2.4. Genetic Algorithm (GA)

GA is used as an optimization technique to solve a bound constrained optimization problem. The basic principle of GA is to randomly vary (mutations) the cutting parameters, and then determine how well they match the fitness function. This process is repeated. The regression model (Equation (1)) developed by response surface methodology was used as the objective function and the upper and lower bound parameters were identified by conducting experiments. GA was used to find the minima of this objective function.

The procedure was as follows:

- A population of n individuals was created. The individuals were initialized with values on the interval of 15 individuals.
- The fitness of the population was evaluated. The fitness of the fittest chromosome was stored in the hall of fame.
- The fittest two chromosomes were carried over to the next generation (elitism).
- Eighty percent of the new generation was created by means of sexual reproduction with tournament selection as follows:
- Ten random individuals (tournament size) were selected from the population.
- Two of the fittest chromosomes were used in the crossover with a randomly generated mask to produce one child chromosome.
- Mutations applied at a probability of pm were applied to the genes of the chromosome.
- The fittest parent and child were carried over to the next generation.
- The remainder of the new generation was created by mutating the least fit chromosomes as follows:
- A random mask was created to determine which genes were to be mutated.
- These genes were mutated by a value on the interval of 15 individuals.

The performance of the GA on this benchmark function was noted. Various parameters such as initial population size, number of generations (iterations), tournament size, and probability of mutation were varied, and the performance of the GA was revaluated. For the code, see Appendix A.

3.2.5. Particle Swarm Algorithm (PSO)

The PSO method is similar to the GA approach, but it calculates a mutation which it then reuses in the next iteration. The regression model (Equation (1)) developed by response surface methodology was used as the objective function and the upper- and lower-bound parameters identified by conducting experiments. PSO was used to find the minima of this objective function.

The procedure was as follows:

- A swarm of n particles was created, representing the cutting parameters. The position of the particles was initialized with random values on the interval of 15 particles. The initial velocity of the particles was set to 0.
- The fitness of the particles was evaluated.
- For each particle, if the fitness calculated was better than its previous personal best, the personal best (y_i) along with its position was updated.
- For each particle, if its personal best was better than the global best ($\hat{y}$), the global best along with its position was updated.
- The velocity(v_i) of each particle (x_i) was updated (for j dimensions) using the following equation:

$$v_{ij}(t+1) = wv_{ij}(t) + c_1 r_1 \left(y_{ij}(t) - x_{ij}(t)\right) + c_2 r_2 (\hat{y_j}(t) - x_{ij}(t)) \quad (2)$$

- where w is the inertia weight, c_1 & c_2 are acceleration constants and r_1 and r_2 are random values on the interval (0;1).

For the code, see Appendix A.

3.2.6. Differential Evolution (DE)

The regression model (Equation (1)) developed by response surface methodology was used as the objective function. The DE method is similar to PSO, but it approaches the randomization slightly differently. The literature shows that it frequently outperforms

PSO [61]. In the present application, a population of n individuals was created. The individuals were initialized with values on the interval (5; 25). DE was used to find the minima of this objective function.

The procedure was as follows:

- The fitness of the population was evaluated. The fitness of the fittest chromosome was stored in the hall of fame.
- The same reproduction operator was used for each individual (target vector) x_i of the population by carrying out the following:
- A trial vector u_i was created from the parent vector and two randomly selected unique individuals x_{i2} and x_{i1}:
- $u_i = x_i + \beta(x_{i2} - x_{i1})$, where β is the scale factor which amplifies the differential variation.
- A binomial crossover was performed between the parent vector and trial vector to produce offspring x_o.
- A randomly selected gene from the trial vector was transferred to the child vector.
- For the rest of the genes, genes from the trial vector were included at a crossover point at a probability, otherwise genes from the parent were included.
- The fitness of the offspring was then evaluated.
- The fitter individual between the parent and offspring was carried over to the next generation.
- Steps 2–5 were repeated for a fixed number of iterations.

For the code, see Appendix A.

4. Results for RSA 443

The surface roughness measurements for the various samples are shown in Table 1.

4.1. Response Transformation Check

According to Table 1, for the results of the experiment, the response surface roughness has a maximum value of 187.18 nm and a minimum value of 14.48 nm. The ratio of maximum value to minimum value is calculated as follows:

$$\frac{187.18}{14.48} = 12.9$$

As the ratio is higher than 10, a transformation will be needed. To select a transformed scale of the model, the technique of Box–Cox plotting was utilized for this analysis; see Figure 1.

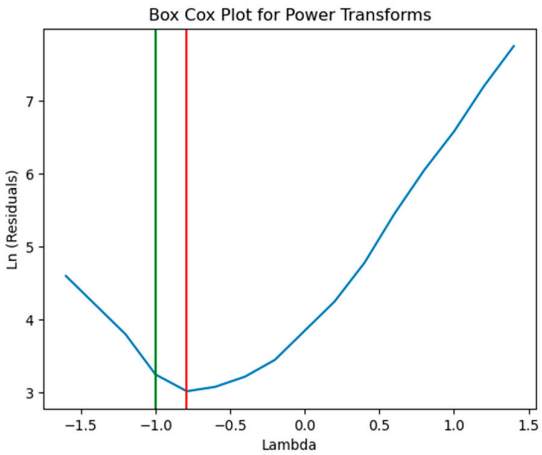

Design Expert Plot: 1.0/(Response 1)

1- Lambda values:

- Current = −1 (green line)
- Best = −0.79 (red line)

2- Recommend transform: Inverse (Lambda = −1)

Figure 1. Box–Cox plotting for transformed scale. Blue line shows residuals, green shows current response, red shows best response.

From Figure 1, an inverse transformation was applied, which formulates a model of the form as follows:

$$y' = \frac{1}{y + k} \quad (3)$$

4.2. Fit Summary

The inverse transformation was used to find a polynomial equation for the relationships between the input parameters and output response surface roughness. The fit summary using a sum of squares sequential model is presented in Table 2.

Table 2. Sequential model sum of squares for surface roughness.

Type of Fit	F-Value	*p*-Value, Prob > F	Lack of Fit, Sum of Squares	Df for Lack of Fit	R-Squared	Evaluation
Linear	24.70	<0.0001	5.541×10^{-4}	9	0.8707	
2FI	0.11	0.9499	5.316×10^{-4}	6	0.8760	
Quadratic	35.01	0.0009	2.409×10^{-5}	3	0.9944	Suggested
Cubic	248.55	0.0040	0.000	0	1.0000	Aliased

The results show that the quadratic fit is the best. It has a good *p*-value (F = 35.01), the lack of fit is small, and its adjusted R-squared value is good. In contrast, the linear model has a moderate adjusted R-squared value, the 2FI model is not statistically significant, and the cubic is aliased.

4.3. Development of a Model for Surface Roughness

There are three input variables (speed, feed, and depth of cut) and one dependent variable of surface roughness. This response surface cannot be graphically visualized in its entirety, but it can be represented piecemeal, as shown in Figure 2.

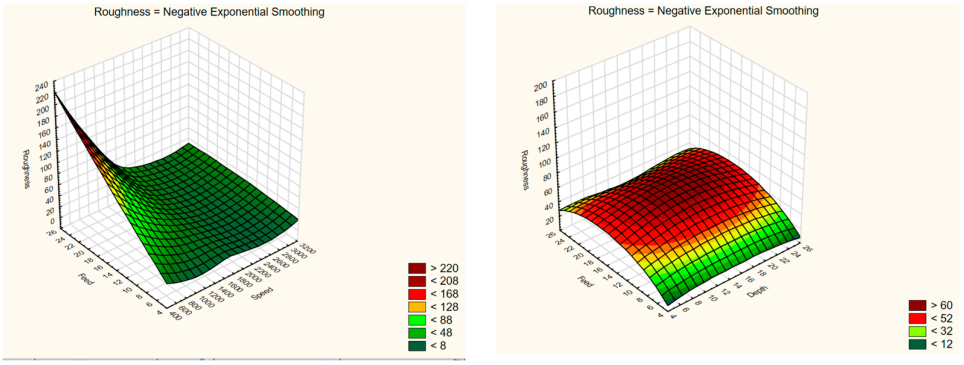

(**a**) (**b**)

Figure 2. Response surface for surface roughness: (**a**) feed and speed, (**b**).

An ANOVA model building was conducted to analyze the relative importance of the model and its terms. The results (F = 98.02, $p < 0.0001$) show a good fit, see Table 3.

Table 3. ANOVA results for the acquired quadratic model.

Source	Sum of Squares	Degree of Freedom	Mean Square	F-Value	*p*-Value Prob > F	Characteristics
Model	4.265×10^{-3}	9	4.736×10^{-4}	98.02	<0.0001	Significant
A-Speed	1.867×10^{-3}	1	1.867×10^{-3}	386.35	<0.0001	Significant
B-Feed	1.865×10^{-3}	1	1.865×10^{-3}	386.03	<0.0001	Significant
C-Depth	6.046×10^{-7}	1	6.046×10^{-7}	0.13	0.7380	
A^2	3.380×10^{-4}	1	3.380×10^{-4}	69.95	0.0004	Significant
B^2	8.091×10^{-5}	1	8.091×10^{-5}	16.75	0.0094	Significant
C^2	7.066×10^{-5}	1	7.066×10^{-5}	14.63	0.0123	Significant
AB	2.905×10^{-7}	1	2.905×10^{-7}	0.060	0.8161	
AC	2.086×10^{-5}	1	2.086×10^{-6}	4.32	0.0923	
BC	1.408×10^{-6}	1	1.408×10^{-6}	0.29	0.6125	
Residuals	2.416×10^{-5}	5	4.832×10^{-6}			
Lack of fit	2.409×10^{-5}	3	8.031×10^{-6}	248.55	0.0040	Significant
Pure Error	6.463×10^{-8}	2	3.231×10^{-8}			
Corr. Total	4.287×10^{-3}	14				

In this section, A, B, A^2, B^2, C^2 are important terms of the model, whereas the other terms are insignificant. Specifically, the terms such as "AB", which correspond to speed x feed, were found to be insignificant and not taken forward. Table 4 shows a high coefficient of determination in that the predicted R-squared is 0.9944 and in good arrangement with the adjusted R-squared of 0.9842. In this analysis, the ratio is 34.038, which indicates an adequate signal against a criteria of a ratio higher than 4 is desired. So, the model may be applied for design space navigation.

Table 4. Summary of regression analysis results.

Std. Dev.	2.198×10^{-3}	R-Squared	0.9944
Mean	0.037	Adj R-Squared	0.9842
C.V	5.96	Pred R-Squared	0.9100
PRESS	3.856×10^{-4}	Adeq Precision	34.038

The model was improved by eliminating all insignificant terms; see Table 5.

Table 5. Results of ANOVA for the modified quadratic model.

Source	Sum of Squares	Degree of Freedom	Mean Square	F-Value	*p*-Value Prob > F	Characteristics
Model	4.265×10^{-3}	9	4.736×10^{-4}	98.02	<0.0001	Significant
A-Speed	1.867×10^{-3}	1	1.867×10^{-3}	386.35	<0.0001	Significant
B-Feed	1.865×10^{-3}	1	1.865×10^{-3}	386.03	<0.0001	Significant
A^2	3.380×10^{-4}	1	3.380×10^{-4}	69.95	0.0004	Significant
B^2	8.091×10^{-5}	1	8.091×10^{-5}	16.75	0.0094	Significant
C^2	7.066×10^{-5}	1	7.066×10^{-5}	14.63	0.0123	Significant
Residuals	2.416×10^{-5}	5	4.832×10^{-6}			
Lack of fit	2.409×10^{-5}	3	8.031×10^{-6}	248.55	0.0040	
Pure Error	6.463×10^{-8}	2	3.231×10^{-8}			
Corr. Total	4.287×10^{-3}	14				

The model takes the form of a second order regressive equation per Equation (4):

$$y = \beta_0 + \sum_i^3 \beta_i x_i + \sum_{i=1}^3 \beta_{ii} x_i^2 + \sum_i \sum_{j=1} \beta_{ij} x_i x_j + \varepsilon \quad (4)$$

where y = the response or output,
x = cutting parameters,
β = the coefficient of estimation which is obtained from RSM analysis.
The resulting numerated model is as follows:

$$\frac{1.0}{R_a} = 0.027756 + 0.0000312344s - 0.0028045f - 0.0000000061230s^2 + 0.0000468123f^2 - 0.00004374d^2 \quad (5)$$

The inverse transformation is as follows:

$$R_a = (0.027756 + 0.0000312344s - 0.0028045f - 0.0000000061230s^2 + 0.0000468123f^2 - 0.00004374d^2)^{-1} \quad (6)$$

where Ra = surface finish or roughness,
s = cutting speed spindle
f = cutting Feed rate
d = cutting depth

4.4. Optimization

The next objective was to determine the optimal process parameters for minimum surface roughness. The response surface (Equation (6)) was used as input to three different AI tools, namely GA, PSO, and DE, to determine optimal process parameters. Cutting speed was the only variable admitted to the optimization study. The other variables were fixed as follows: cutting feed rate (f = 5 mm/min) and cutting depth (d = 15 μm). Implementing codes of these functions was written in MATLAB (version 2018). For the code, see Appendix A.

A convergence study was undertaken, details of which are shown in Appendix B. The results are shown in Table 6.

Table 6. Predicted roughness using optimization methods.

	Function	Cutting Speed(rpm)	Iterations or Generations		
			150	500	1500
GA	Ra_s500	500	-	-	-
	Ra_s1500	1500	44.21 nm	-	22.15 nm
	Ra_s3000	3000	-	14.02 nm	-
PSO	Ra_s500	500	-	-	-
	Ra_s1500	1500	-	-	-
	Ra_s3000	3000	211.0 nm	121.84 nm	211.0 nm
DE	Ra_s500	500	-	-	-
	Ra_s1500	1500	-	37.38 nm	-
	Ra_s3000	3000	36.28 nm	-	67.87 nm

The best (lowest) surface roughness result of 14.02 nm was gained with GA, which identified a minimum value to Ra (14.48 nm) at a cutting speed of 3000 rpm, with fixed variables of a cutting feed of 5 mm/min and cutting depth of 15 μm.

The mean absolute percentage error (MAPE) was determined by comparing the predicted surface roughness in Table 6 to the experimental data in Table 1, interpolating the latter where necessary.

$$MAPE = \frac{1}{k}\sum_{i=1}^{k} \left| \frac{Ram - Rap, i}{Ram} \right| 100 \quad (7)$$

where

k = the total number of measurements,

i = the estimated measurement for a specific run,

Ram = the measured surface roughness for a specific run

Rap, i = the predicted surface roughness for a specific run

The GA error was 3.2%. This discrepancy arises from the imperfections of the curve fitting and the GA method. Assuming that this same error applies to the process parameters in general, then the recommended cutting parameters are a feed rate of 4.84 mm/min, cutting depth of 14.52 μm, and cutting speed of 3000 rpm.

5. Discussion

5.1. Findings

The main findings are the identification of a specific set of process parameters for minimizing the surface roughness on diamond machined aluminium alloy RSA 443, namely a feed rate of 4.84 mm/min, a cutting depth of 14.52 μm, and a cutting speed of 3000 rpm. Note that feed rate was at the lowest setting, cutting depth was in the middle of the range, and rotational speed was at the maximum.

This result is counter intuitive. Usually, a smaller depth of cut results in a better surface roughness. The current results show that a depth of about 15 μm is optimal—the smallest value tested was 5 μm. Note that the cutting speed was high, and the feed rate was consistent with other applications of diamond turning.

A possible physical explanation for this is as follows. From a materials removal perspective, the extreme combination of low feed rate and high rotational speed corresponds to a situation where a very axially thin annular ring of material is removed. The thinness of the ring means that there is a reduced plastic distortion of the substrate when the material is removed. It also means that the tip of the tool travels only slowly in the axial direction, thus providing less opportunity for axial striations to develop. The findings show that the genetic algorithm optimization performed better than the PSO and DE. Possible reasons for this are (1) the GA is a stochastic attempt to optimally solve a known problem and (2) the underlying physical phenomenon may include a global optimum location which suits the GA approach.

The RSA group of materials has a much finer microstructure than the already fine structure of the 6000 precipitation hardening aluminium alloys. For the RSA materials, the alloying elements change the molecular dynamics, which in turn affects the surface roughness [62]. The RSA process results in a variable solidification rate across the spun section, with the alloying particles being oriented with the aluminium matrix [63]. Hence, the microstructures of a piece of RSA material are both complex in terms of the grain structures, and inhomogeneous through the section. The microstructural configuration at the point of machining potentially has anisotropy mechanical properties [28]. It is to be expected that this will affect the cutting behavior by changing the tool-cutting dynamics (including chip formation) and hence affect the surface roughness. However, this complex interaction is only beginning to be explored; for a review of simulation of the effect on lattice deformation and crack propagation (at the atomic scale) on chip formation, see [28].

5.2. Implications for Industry Practitioners

Potential implications are that optical product performance may be enhanced. Surface roughness optimization ensures that components and products have the right texture and smoothness required for their intended functions. For example, in manufacturing mechanical parts, optimizing surface roughness can reduce friction, wear, and noise, leading to improved overall performance and longevity.

While the work was primarily motivated by optical applications, there are other potential uses for minimized surface roughness. In industries where precision is crucial, such as aerospace and automotive, optimizing surface roughness can enhance the efficiency of

moving parts and reduce energy consumption. There are also potential implications for surface protection: controlled surface roughness can alter the corrosion and wear effects, hence enhancing the durability and reliability of products, especially in harsh environments or under extreme conditions.

5.3. Limitations of the Study

Surface roughness can be influenced by various factors, not all of which were included in the study. These other variables include machine conditions, ambient thermal control, the acoustic and vibrational environment, and operator skill. The present study assumed these were already all in control, whereas in practice, these environmental parameters may not be. The present study also did not examine the repeatability across different batches of raw material or from different suppliers. Furthermore, the number of samples was relatively limited—only a single data point was collected for each combination of process settings; hence, it was not possible to create a confidence interval over the response surface. This is to say that the fitness function was deterministic. In addition, a depth of cut less than 5 μm was not investigated.

5.4. Implications for Further Research

A potentially interesting area for further exploration could be the real-time monitoring of surface roughness, and dynamic control thereof. This would require the development of sensors and control techniques. This could ensure consistent quality and reduce scrap rates. Another line of research could be to better understand the underlying phenomenon of metal removal and surface roughness. The current model is based purely on fit and produces a second order regressive equation; however, it does not address the ontological question of why the relationship should have these squared terms. A deeper ontological model has the potential to lead to the development of new materials and alloys that more readily allow the manufacture of the desired surface roughness properties.

6. Conclusions

The surface roughness machinability of RSA443 in single-point diamond turning was primarily determined by cutting speed, and secondly, cutting feed rate, with cutting depth being less important. The optimal conditions for the best Ra = 14.02 nm were found to be at the maximum rotational speed of 3000 rpm, cutting feed rate of 4.84 mm/min, and depth of cut of 14.52 μm with an optimizing error of 3.2%.

Regarding optimization techniques, genetic algorithm performed best, then differential evolution, and finally particle swarm optimization.

This study makes a contribution of determining optimal machining parameters for RSA443, and shows a method using artificial intelligence whereby this can relatively quickly be determined for other materials and machining processes.

Author Contributions: Conceptualization: G.M.T.; formal analysis: G.M.T.; investigation: G.M.T.; methodology: G.M.T.; software: G.M.T.; validation: G.M.T.; visualization: G.M.T.; interpretation of data: G.M.T. and D.P.; writing—original draft: G.M.T.; writing—review and editing: G.M.T. and D.P. All authors have read and agreed to the published version of the manuscript.

Funding: This research received no external funding.

Data Availability Statement: See Appendix A for code. No additional data available.

Conflicts of Interest: The authors declare no conflict of interest.

Appendix A. Code Statement (MATLAB)

Fitness functions

- *SurfaceRoughness_s500*

```
function [y] = SurfaceRoughness_s500(x)
```

```
dim = 15; %Population size
ra = 0;
for i = 1:(dim-1)
a = x(i);
b = x(i + 1);
ra = ra + (0.027756 + 3.12344E-005*500 − 2.80457E-003*a-6.12306E-009 * 500. ^2 +
4.68123E-005 * a.^2 − 4.37473E-005 * b.^2).^(−1);
end
y = ra;
```

- *SurfaceRoughness_s1750*

```
function [y] = SurfaceRoughness_s1750(x)
dim = 15; %Population size
ra = 0;
for i = 1:(dim-1)
a = x(i);
b = x(i + 1);
ra = ra + (0.027756 + 3.12344E-005*1750 −2.80457E-003*a − 6.12306E-009 * 1750. ^2 +
4.68123E-005*
a.^2 − 4.37473E-005 * b.^2). ^ (−1);
end
y = ra;
```

- *SurfaceRoughness_s3000*

```
function [y] = SurfaceRoughness_s3000(x)
dim = 15; %Population size
ra = 0;
for i = 1:(dim-1)
a = x(i);
b = x(i + 1);
ra = ra + (0.027756 + 3.12344E-005*3000 −2.80457E-003*a − 6.12306E-009 * 3000. ^2 +
4.68123E-005*
a.^2 − 4.37473E-005 * b.^2). ^ (−1);
end
y = ra;
```

GA code

```
%Surface Roughness: Genetic Algorithm (GA)
clc;
clear;
%Setting up Parameters
n = 15; %Population size
iterations = 500; %Number of iterations/generations
%Chromosomes have 15 genes
%Matrix to store population and fitness for each objective function.
pop1 = zeros(n,16); %SurfaceRoughness_s500
pop2 = zeros(n,16); %SurfaceRoughness_s1750
pop3 = zeros(n,16); %SurfaceRoughness_s3000
%Matrix to store elite of each pop for each iteration (Hall of Fame)
el1 = zeros(iterations,16);
el2 = zeros(iterations,16);
el3 = zeros(iterations,16);
%Population initialized with random values on interval
init = 20;
for i = 1:n
```

```
for j = 1:15
pop1(i,j) = 5+init*rand(1);
pop2(i,j) = 5+init*rand(1);
pop3(i,j) = 5 + init*rand(1);
end
end
%Outerloop of iterations
for iter = 1:iterations
%Use objective function to determine fitness of populations
for i = 1:n
pop1(i,16) = SurfaceRoughness_s500(pop1(i,1:15));
pop2(i,16) = SurfaceRoughness_s1750(pop2(i,1:15));
pop3(i,16) = SurfaceRoughness_s3000(pop3(i,1:15));
end
%Sort population is ascending order of fitness
pop1 = sortrows(pop1,16);
pop2 = sortrows(pop2,16);
pop3 = sortrows(pop3,16);
%Store elite chromosome from each generation
el1(iter,1:16) = pop1(1,1:16);
el2(iter,1:16) = pop2(1,1:16);
el3(iter,1:16) = pop3(1,1:16);
%Reproduction
if (iter ~= iterations)
%Matrix to store new population
newpop1 = zeros(n,16);
newpop2 = zeros(n,16);
newpop3 = zeros(n,16);
iasex = 10; %Number of asexual reproductions
isex = n-iasex; %Number of sexual reproductions
tsize =15; %Number of individuals in tournament
pm = 0.000075;
%Use elitism to keep top two chromosomes from each population
newpop1(1,1:16) = pop1(1,1:16);
newpop1(2,1:16) = pop1(2,1:16);
newpop2(1,1:16) = pop2(1,1:16);
newpop2(2,1:16) = pop2(2,1:16);
newpop3(1,1:16) = pop3(1,1:16);
newpop3(2,1:16) = pop3(2,1:16);
%Sexual Reproduction with tournament selection
for b = 1:3
switch b
case 1 %SurfaceRoughness_s500
pop = pop1;
newpop = newpop1;
case 2 %SurfaceRoughness_s1750
pop = pop2;
newpop = newpop2;
case 3 %SurfaceRoughness_s3000
pop = pop3;
newpop = newpop3;
end
for i = 3:isex
if(mod(i,2) ~= 0)
```

```
%Tournament for pop1
tourn = zeros(tsize,16);
for j = 1:tsize
c = ceil(rand(1)*n);
tourn(j,1:16) = pop(c,1:16);
end
tourn = sortrows(tourn,16);
p1 = tourn(1,1:16);
p2 = tourn(2,1:16);
c = zeros(1,16);
geneselect = round(rand(1,15));
for k = 1:15
if (geneselect == 1)
c(k) = p1(k);
else
c(k) = p2(k);
end
%Mutate gene
mut = rand(1);
if (mut < pm)
c(k) = c(k) + (−0.5 +rand(1))*c(k);
end
end
newpop(i,1:15) = c(1:15); %Add child to newpop
newpop(i + 1,1:15) = p1(1:15); %Add fitest child to newpop
end
end
%At this stage population size is equal to isex
%Asexual reproduction of weakest chromosomes
pma = 0.0035; %Prob of mutation in asexual reproduction
for i = isex + 1:n
geneselect = round(rand(1,15));
c = pop(i,1:15);
for k = 1:15
if(geneselect == 1)
c(k) = −5 + 2*init*rand(1); %-5 + 2*init*rand(1) or c(k) + (−1 + rand(1))*c(k);
end
end
newpop(i,1:15) = c(1:15);
end
pop = newpop;
switch b
case 1 %SurfaceRoughness_s500
pop1 = pop;
newpop1 = newpop;
case 2 %SurfaceRoughness_s1750
pop2 = pop;
newpop = newpop2;
case 3 %SurfaceRoughness_s3000
pop3 = pop;
newpop3 = newpop;
end
end
end
```

```
iter
end
```

PSO code:

```
%Surface Roughness: Particle Swarm Optimization
clc;
clear;
n = 15; %Swarm size
iterations = 100; %Number of iterations
%Acceleration and inertia constants
c1 = 5.0;
c2 = 1.0;
w = 0.5; %Best so far c2,c2,w = 2,2,0.5
%Matrix to store individual data [xi(1:30),vi(31:60),Bi(61),yj(62:91),Bj(92)]
pop1 = zeros(n,92); %SurfaceRoughness_s500
pop2 = zeros(n,92); %SurfaceRoughness_s1750
pop3 = zeros(n,92); %SurfaceRoughness_s3000
%Matrix to store elite of each swarm for each iteration
el1 = zeros(iterations,16);
el2 = zeros(iterations,16);
el3 = zeros(iterations,16);
%Vector to store Global best of each swarm
gb1 = zeros(1,16);
gb2 = zeros(1,16);
gb3 = zeros(1,16);
%Initialize gb*(16) to 999999
gb1(16) = 999999;
gb2(16) = 999999;
gb3(16) = 999999;
%Population initialized with random values on interval
init = 20;
for i = 1:n
for j = 1:15
pop1(i,j) = 5+init*rand(1);
pop2(i,j) = 5+init*rand(1);
pop3(i,j) = 5+init*rand(1);
end
end
%Outer loop
for iter = 1: iterations
for i = 1:n
%Perform objective functions
pop1(i,61) = SurfaceRoughness_s500(pop1(i,1:15));
pop2(i,61) = SurfaceRoughness_s1750(pop2(i,1:15));
pop3(i,61) = SurfaceRoughness_s3000(pop3(i,1:15));
end
%Do for each population
for b = 1:3
switch b
case 1 %SurfaceRoughness_s500
pop = pop1;
el = el1;
gb = gb1;
case 2 %SurfaceRoughness_s1750
```

```
pop = pop2;
el = el2;
gb = gb2;
case 3 %SurfaceRoughness_s3000
pop = pop3;
el = el3;
gb = gb3;
end
%Sort Swarm in ascending order of objective functions or benchmark function values
pop = sortrows(pop,61);
%Check for global best
if(pop(1,61) < gb(16))
b(1,1:15) = pop(1,1:15);
gb(16) = pop(1,61);
end
%Store Global best in hall of fame
el(iter,1:16) = gb(1:16);
if(iter~= iterations)
for i = 1:n
%Check for personal best
if((pop(i,61) < pop(i,92))||iter == 1)
pop(i,62:76) = pop(i,1:15);
pop(i,92) = pop(i,16);
end
%Calculate velocity of particle
for j = 16:30
pop(i,j) = w*pop(i,j) + (c1*rand(1)*(pop(i,j + 16)-pop(i,j-15))) + (c2*rand(1)*(el(iter,j-
15)-pop(i,j-15)));
end
%Update position of particle
for j = 1:15
pop(i,j) = pop(i,j) + pop(i,j + 15);
end
end
end
switch b
case 1 %SurfaceRoughness_s500
pop1 = pop;
el1 = el;
gb1 = gb;
case 2 %SurfaceRoughness_s1750
pop2 = pop;
el2 = el;
gb2 = gb;
case 3 %SurfaceRoughness_s3000
pop3 = pop;
el3 = el;
gb3 = gb;
end
end
iter
end
```

DE code:

```
%Surface Roughness: Differential Evolution (DE)
clc;
clear;
%Setting up Parameters
n = 15; %Population size
iterations = 2000; %Number of iterations/generations
B = 0.00075; %Scale
pm = 0.000035; %probability of crossover
%Chromosomes have 15 genes
%Matrix to store population and fitness for each or objective function or benchmark function.
pop1 = zeros(n,16); %SurfaceRoughness_s500
pop2 = zeros(n,16); %SurfaceRoughness_s1750
pop3 = zeros(n,16); %SurfaceRoughness_s3000
%Matrix to store elite of each pop for each iteration (Hall of Fame)
el1 = zeros(iterations,16);
el2 = zeros(iterations,16);
el3 = zeros(iterations,16);
%Population initialized with random values on interval
init = 20;
for i = 1:n
for j = 1:15
pop1(i,j) = 5+init*rand(1);
pop2(i,j) = 5+init*rand(1);
pop3(i,j) = 5+init*rand(1);
end
end
%Outer loop of iterations
for iter = 1: iterations
for i = 1:n
pop1(i,16) = SurfaceRoughness_s500(pop1(i,1:15));
pop2(i,16) = SurfaceRoughness_s1750(pop2(i,1:15));
pop3(i,16) = SurfaceRoughness_s3000(pop3(i,1:15));
end
%Matrix to store new population
newpop1 = zeros(n,16);
newpop2 = zeros(n,16);
newpop3 = zeros(n,16);
%DE loop (Mutation and crossovers)
for b = 1:3
switch b
case 1 %SurfaceRoughness_s500
pop = pop1;
newpop = newpop1;
el = el1;
case 2 %SurfaceRoughness_s1750
pop = pop2;
newpop = newpop2;
el = el2;
case 3 %SurfaceRoughness_s3000
pop = pop3;
newpop = newpop3;
el = el3;
end
```

```
%Sort population is ascending order of fitness
pop = sortrows(pop,16);
%Store elite chromosome from each generation
el(iter,1:16) = pop(1,1:16);
if(iter~= iterations)
for i = 1:n
xi = pop(i,1:16); %Target Vector
np1 = ceil(rand(1)*n); %Index of parent1
np2 = ceil(rand(1)*n); %Index of parent2
while(np1 = =np2) %Ensure parents are unique
np2 = ceil(rand(1)*n);
end
p1 = pop(np1,1:15);
p2 = pop(np2,1:15);
ui = zeros(1,16); %Create Trial Vector
for j = 1:15
ui(j) = xi(j) + (B*(p1(j)-p2(j)));
end
xo = xi; %Offspring Vector
keep = ceil(rand(1)*15); %Gene to include of trial vector
xo(keep) = ui(keep); %Crossover
for j = 1:15
prob = rand(1);
if (prob < pm && j~= keep)
xo(j) = ui(j);
end
end
switch b %Determine Fitness
case 1
xo(16) = SurfaceRoughness_s500(xo(1:15));
case 2
xo(16) = SurfaceRoughness_s1750(xo(1:15));
case 3
xo(16) = SurfaceRoughness_s3000(xo(1:15));
end
%Keep offspring if fitter, else keep target
if(xo(16) < xi(16))
newpop(i,1:16) = xo;
else
newpop(i,1:16) = xi;
end
end
pop = newpop;
end
switch b
case 1 %SurfaceRoughness_s500
pop1 = pop;
newpop1 = newpop;
el1 = el;
case 2 %SurfaceRoughness_s1750
pop2 = pop;
newpop = newpop2;
el2 = el;
case 3 %SurfaceRoughness_s3000
```

```
pop3 = pop;
newpop3 = newpop;
el3 = el;
end
end
iter
end
```

Appendix B. Convergence Results

The GA was able to converge the Ra_s1750 function to its minimum after approximately 150 iterations and 1500 iterations, following successive values of 44.21 nm and 22.15 nm. Also, the Ra_s3000 function converged slower than other benchmark functions for all the optimization algorithms accordingly; see Figures A1c,f, A2, and A3. The longer convergence time compared to the other benchmark functions is attributed to the high number of local minima in the Ra_s3000 function and its minimum (14.02 nm).

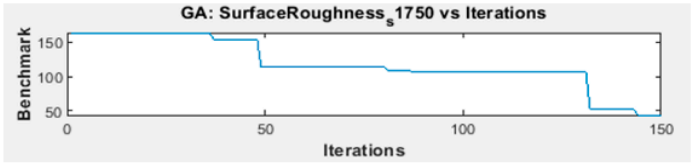

Minimum value of 44.21nm with 150 iterations and 1750 rpm

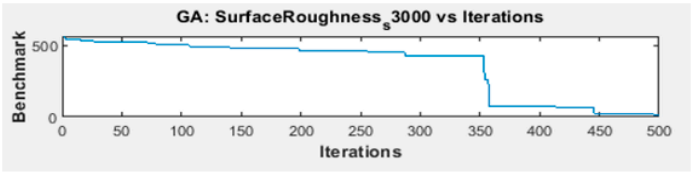

Minimum value of 14.02nm with 500 iterations and 3000rpm

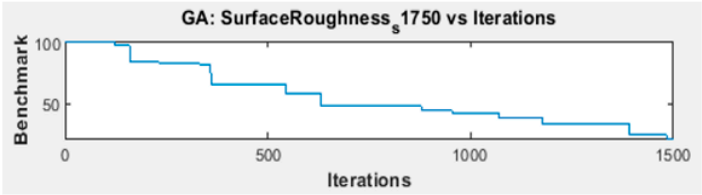

Minimum value of 22.15nm with 1500 iterations and 1750rpm

Figure A1. Convergence results for GA.

The PSO was able to converge the Ra_s3000 function to its minimum after all approximately selected iterations; see Figure A2. These selected iterations were 150, 500, and 1500 with their successive benchmark values: 211.00 nm, 121.84 nm, and 211nm; however, the rate of convergence is higher than for GA and DE.

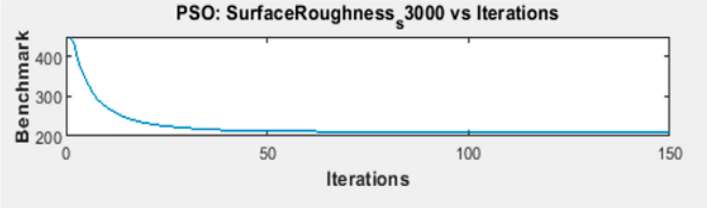

Minimum value of 211.00nm with 150 iterations and 3000rpm

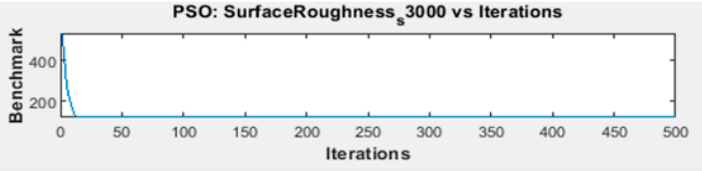

Minimum value of 121.84nm with 500 iterations and 3000rpm

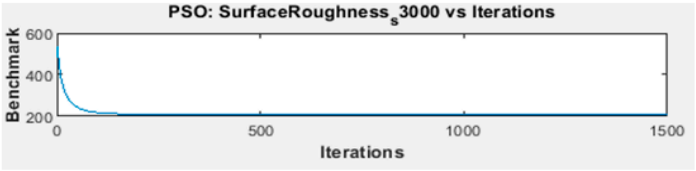

Minimum value of 211nm with 1500 iterations and 3000rpm

Figure A2. Convergence results PSO.

The DE took the longest to converge the Ra_s3000 function to its minimum. It took approximately 150 iterations; see Figure A3. The DE was only able to minimize the Ra_s3000 function to 36.28nm and 67.87nm for 150 iterations and 1500 iterations. Additionally, it converged the Ra_s1750 function to 37.38 nm after 500 iterations.

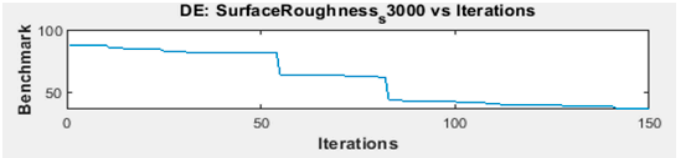

Minimum value of 36.28nm with 150 iterations and 3000rpm

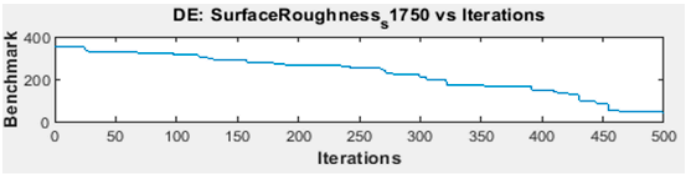

Minimum value of 37.38nm with 500 iterations and 1750rpm

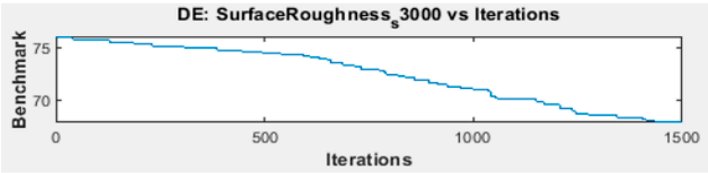

Minimum value of 67.87nm with 1500 iterations and 3000rpm

Figure A3. Convergence results for DE.

References

1. Sanger, G.M. Optical fabrication technology, the present and future. In *Contemporary Methods of Optical Manufacturing and Testing*; International Society for Optics and Photonics: Washington, DC, USA, 1983.
2. Al-Homoud, M.S., Performance characteristics and practical applications of common building thermal insulation materials. *Build. Environ.* **2005**, *40*, 353–366.
3. Routara, B.; Bandyopadhyay, A.; Sahoo, P. Roughness modeling and optimization in CNC end milling using response surface method: Effect of workpiece material variation. *Int. J. Adv. Manuf. Technol.* **2009**, *40*, 1166–1180.
4. Abbas, A.T.; Pimenov, D.Y.; Erdakov, I.N.; Taha, M.A.; El Rayes, M.M.; Soliman, M.S. Artificial intelligence monitoring of hardening methods and cutting conditions and their effects on surface roughness, performance, and finish turning costs of solid-state recycled Aluminum alloy 6061 chips. *Metals* **2018**, *8*, 394.
5. Otieno, T.; Abou-El-Hossein, K.; Hsu, W.Y.; Cheng, Y.C.; Mkoko, Z. Surface roughness when diamond turning RSA 905 optical aluminium. In Proceedings of the SPIE Optical Engineering + Applications, San Diego, CA, USA, 9–13 August 2015; Volume 9575.
6. Gregoire, M.T. Optimization of Surface Roughness of Alumimium Grade (RSA 443) in Diamond Tool Turning. Master's Thesis, Nelson Mandela University, George, South Africa, 2021.
7. Gao, B.; Zhao, H.; Peng, L.; Sun, Z. A review of research progress in selective laser melting (SLM). *Micromachines* **2022**, *14*, 57. https://doi.org/10.3390/mi14010057.
8. Zhang, L.; Sato, Y.; Yan, J. Optimization of fast tool servo diamond turning for enhancing geometrical accuracy and surface quality of freeform optics. *J. Adv. Mech. Des. Syst. Manuf.* **2023**, *17*, JAMDSM0012. https://doi.org/10.1299/jamdsm.2023jamdsm0012.
9. Hatefi, S.; Abou-El-Hossein, K. Review of magnetic-assisted single-point diamond turning for ultra-high-precision optical component manufacturing. *Int. J. Adv. Manuf. Technol.* **2022**, *120*, 1591–1607. https://doi.org/10.1007/s00170-022-08791-3.
10. Aditi, G.; Daren, D.; Isabel, K.; Andrew, S.; Renate, K.; Deno, S.; Pavl, Z.; Nick, M.; Michael, G. Optics testing for SCALES. In Proceedings of the SPIE Optical Engineering + Applications, San Diego, CA, USA, 20–25 August 2023. https://doi.org/10.1117/12.2677808.
11. Qiu, J. Fundamental research on machining performance of diamond wire sawing and diamond wire electrical discharge sawing quartz glass. *Ceram. Int.* **2022**, *48*, 24332–24345. https://doi.org/10.1016/j.ceramint.2022.04.327.
12. Wang, J.; Wen, Y.; Han, J.; Ma, S.; Zhang, G. A novel tool wear suppression method for polycrystalline diamond by applying magnetic field in turning of ferrous materials. *Proc. Inst. Mech. Eng. Part B J. Eng. Manuf.* **2022**, *236*, 1772–1781. https://doi.org/10.1177/09544054221099268.
13. Gupta, A.; Saini, A.; Khatri, N.; Juyal, A. Review of single-point diamond turning process on IR optical materials. *Mater. Today Proc.* **2022**, *69*, 435–440. https://doi.org/10.1016/j.matpr.2022.09.073.
14. La Monaca, A.; Murray, J.W.; Liao, Z.; Speidel, A.; Robles-Linares, J.A.; Axinte, D.A.; Hardy, M.C.; Clare, A.T. Surface integrity in metal machining-Part II: Functional performance. *Int. J. Mach. Tools Manuf.* **2021**, *164*, 103718. https://doi.org/10.1016/j.ijmachtools.2021.103718.
15. Wang, L.; Ge, S.; Si, H.; Yuan, X.; Duan, F. Roughness control method for five-axis flank milling based on the analysis of surface topography. *Int. J. Mech. Sci.* **2020**, *169*, 105337. https://doi.org/10.1016/j.ijmecsci.2019.105337.
16. Ning, P.; Zhao, J.; Ji, S.; Li, J.; Dai, H. Simulation and experiment on surface topography of complex surface in single point diamond turning based on determined tool path. *Int. J. Adv. Manuf. Technol.* **2021**, *113*, 2555–2562. https://doi.org/10.1007/s00170-021-06671-w.
17. Li, D.; Qiao, Z.; Walton, K.; Liu, Y.; Xue, J.; Wang, B.; Jiang, X. Theoretical and experimental investigation of surface topography generation in slow tool servo ultra-precision machining of freeform surfaces. *Materials* **2018**, *11*, 2566. https://doi.org/10.3390/ma11122566.
18. Hatefi, S.; Abou-El-Hossein, K. Review of hybrid methods and advanced technologies for in-process metrology in ultra-high-precision single-point diamond turning. *Int. J. Adv. Manuf. Technol.* **2020**, *111*, 427–447. https://doi.org/10.1007/s00170-020-06106-y.
19. Chen, Z.; Chen, G.; Yu, Z.; Huang, J.; Wei, H. Status of research on non-conventional technology assisted single-point diamond turning. *Nanotechnol. Precis. Eng. NPE* **2023**, *6*, 035002. https://doi.org/10.1063/10.0019549.
20. Nair, A.; Kumanan, S.; Prakash, C.; Mohan, D.G.; Sxena, K.K.; Kumar, S.; Kumar, G. Research developments and technological advancements in conventional and non-conventional machining of superalloys—A review. *J. Adhes. Sci. Technol.* **2023**, *37*, 3053–3124. https://doi.org/10.1080/01694243.2023.2186202.
21. Chopade, S.R.; Barve, S.B. A single point diamond turning and integrated sensory system in nano machining: A survey, research issues and challenges. *Mater. Today Proc.* **2023**, 2214–7853. https://doi.org/10.1016/j.matpr.2023.09.070.
22. Czerwinski, F.J.M. Thermal stability of aluminum alloys. *Materials* **2020**, *13*, 3441. https://doi.org/10.3390/ma13153441.
23. Kareem, A.; Qudeiri, J.A.; Abdudeen, A.; Ahammed, T.; Ziout, A. A review on AA 6061 metal matrix composites produced by stir casting. *Materials* **2021**, *14*, 175. https://doi.org/10.3390/ma14010175.
24. Zhang, P.; Tan, J.; Tian, Y.; Yan, H.; Yu, Z. Research progress on selective laser melting (SLM) of bulk metallic glasses (BMGs): A review. *Int. J. Adv. Manuf. Technol.* **2021**, *118*, 2017–2057. https://doi.org/10.1007/s00170-021-07990-8.
25. Nikanorov, S.; Osipov, V.; Regel, L. Structural and mechanical properties of directionally solidified Al-Si Alloys. *J. Mater. Eng. Perform.* **2019**, *28*, 7302–7323. https://doi.org/10.1007/s11665-019-04414-3.

26. Chaieb, O.; Olufayo, O.A.; Songmene, V.; Jahazi, M. Investigation on surface quality of a rapidly solidified Al–50% Si alloy component for deep-space applications. *Materials* **2020**, *13*, 3412. https://doi.org/10.3390/ma13153412.
27. Hweju, Z.; Abou-El-Hossein, K. Surface roughness prediction based on acoustic emission signals in high-precision diamond turning of rapidly solidified optical aluminum grade (RSA443). *Key Eng. Mater.* **2020**, *841*, 363–368. https://doi.org/10.4028/www.scientific.net/KEM.841.363.
28. Zhao, L.; Zhang, J.; Zhang, J.; Dai, H.; Hartmaier, A.; Sun, T. Numerical simulation of materials-oriented ultra-precision diamond cutting: Review and outlook. *Int. J. Extrem. Manuf.* **2023**, *5*, 022001. https://doi.org/10.1088/2631-7990/acbb42.
29. Abou-El-Hossein, K.; Olufayo, O.; Mkoko, Z. Diamond tool wear during ultra-high precision machining of rapidly solidified aluminium RSA 905. *Wear* **2013**, *302*, 1105–1112. https://doi.org/10.1016/j.wear.2012.12.060.
30. Mkoko, Z.; Abou-El-Hossein, K. Aspects of ultra-high-precision diamond machining of RSA 443 optical aluminium. In Proceedings of the SPIE Optical Engineering + Applications, San Diego, CA, USA, 9–13 August 2015; Volume 9575.
31. Musavi, S.H.; Davoodi, B.; Eskandari, B. Evaluation of surface roughness and optimization of cutting parameters in turning of AA2024 alloy under different cooling-lubrication conditions using RSM method. *J. Cent. South Univ.* **2020**, *27*, 1714–1728. https://doi.org/10.1007/s11771-020-4402-2.
32. Guo, J.; Zhang, J.; Wang, H.; Liu, K.; Kumar, A.S. *S*urface quality characterisation of diamond cut V-groove structures made of rapidly solidified aluminium RSA-905. *Precis. Eng.* **2018**, *53*, 120–133. https://doi.org/10.1016/j.precisioneng.2018.03.004.
33. Saini, V.; Sharma, D.; Kalla, S.; Chouhan, T. Optimisation of process parameter in ultra-precision diamond turning of polycarbonate material. In Proceedings of the International Conference on Manufacturing Excellence MANFEX, Noida, India, 29–30 March 2012.
34. Cheung, C.F.; Lee, W.B. A theoretical and experimental investigation of surface roughness formation in ultra-precision diamond turning. *Int. J. Mach. Tools Manuf.* **2000**, *40*, 979–1002. https://doi.org/10.1016/S0890-6955(99)00103-0.
35. Wu, D.; Zhang, P.; Wang, H.; Qiao, Z.; Wang, B. Effect of cutting parameters on surface quality during diamond turning of micro-prism array. *Proc. Inst. Mech. Eng. Part B J. Eng. Manuf.* **2017**, *231*, 555–561.
36. He, C.; Zong, W.; Cao, Z.; Sun, T. Theoretical and empirical coupled modeling on the surface roughness in diamond turning. *Mater. Des.* **2015**, *82*, 216–222. https://doi.org/10.1016/j.matdes.2015.05.058.
37. Baş, D.; Boyacı, I.H. Modeling and optimization I: Usability of response surface methodology. *J. Food Eng.* **2007**, *78*, 836–845.
38. Morshedi, A.; Akbarian, M. Application of response surface methodology: Design of experiments and optimization: A mini review. *J. Fundam. Appl. Life Sci.* **2014**, *54*, 2434–2439.
39. Azam, M.; Jahanzaib, M.; Wasim, A. Surface roughness modeling using RSM for HSLA steel by coated carbide tools. *Int. J. Adv. Manuf. Technol.* **2015**, *78*, 1031–1041.
40. Asiltürk, I.; Neşeli, S.; Ince, M.A. Optimisation of parameters affecting surface roughness of Co28Cr6Mo medical material during CNC lathe machining by using the Taguchi and RSM methods. *Measurement* **2016**, *78*, 120–128. https://doi.org/10.1016/j.measurement.2015.09.052.
41. Xiao, M.; Shen, X.; Ma, Y.; Yang, F.; Gao, N.; Wei, W.; Wu, D. Prediction of surface roughness and optimization of cutting parameters of stainless steel turning based on RSM. *Math. Probl. Eng.* **2018**, *2018*, 9051084. https://doi.org/10.1155/2018/9051084.
42. Kumar, R.; Channi, A.S.; Kaur, R.; Sharma, S.; Grewal, J.S.; Singh, S.; Verma, A.; Haber, R. Exploring the intricacies of machine learning-based optimization of electric discharge machining on squeeze cast TiB2/AA6061 composites: Insights from morphological, and microstructural aspects in the surface structure analysis of recast layer formation and worn-out analysis. *J. Mater. Res. Technol.* **2023**, *26*, 8569–8603. https://doi.org/10.1016/j.jmrt.2023.09.127.
43. Venkata Rao, K.; Murthy, P. Modeling and optimization of tool vibration and surface roughness in boring of steel using RSM, ANN and SVM. *J. Intell. Manuf.* **2018**, *29*, 1533–1543. https://doi.org/10.1007/s10845-016-1197-y.
44. Sims, K. Evolving 3D morphology and behavior by competition. *Artif. Life* **1994**, *1*, 353–372.
45. Forrest, S. Genetic algorithms: Principles of natural selection applied to computation. *Science* **1993**, *261*, 872–878.
46. Suresh, P.; Rao, P.V.; Deshmukh, S. A genetic algorithmic approach for optimization of surface roughness prediction model. *Int. J. Mach. Tools Manuf.* **2002**, *42*, 675–680.
47. Gill, D.S.K.; Gupta, M.; Gupta, M.; Satsangi, P.S. A genetic algorithmic approach for optimization of surface roughness prediction model in turning using UD-GFRP composite. *Indian J. Eng. Mater. Sci.* **2012**, *19*, 386–396.
48. Sardinas, R.Q.; Santana, M.R.; Brindis, E.A. Genetic algorithm-based multi-objective optimization of cutting parameters in turning processes. *Eng. Appl. Artif. Intell.* **2006**, *19*, 127–133. https://doi.org/10.1016/j.engappai.2005.06.007.
49. Seeman, M.; Kanagarajan, D.; Sivaraj, P.; Seetharaman, R.; Devaraju, A. Optimization through NSGA-II during machining of A356Al/20% SiCp metal matrix composites using PCD Tool. In Proceedings of the IOP Conference Series: Materials Science and Engineering, Kanchipuram, India, 8–10 May 2019; IOP Publishing: Bristol, UK, 2019. https://doi.org/10.1088/1757-899X/574/1/012008.
50. Lu, Z.S.; Wang, M.H. Optimization of cutting conditions in ultra-precision turning based on mixed genetic-simulated annealing algorithm. *Key Eng. Mater.* **2006**, *315*, 617–622. https://doi.org/10.4028/www.scientific.net/KEM.315-316.617.
51. Xie, N.; Zhou, J.; Zheng, B. An energy-based modeling and prediction approach for surface roughness in turning. *Int. J. Adv. Manuf. Technol.* **2018**, *96*, 2293–2306. https://doi.org/10.1007/s00170-018-1738-y.
52. Klancnik, S.; Brezocnik, M.; Balic, J.; Karabegovic, I. Programming of CNC milling machines using particle swarm optimization. *Mater. Manuf. Process.* **2013**, *28*, 811–815. https://doi.org/10.1080/10426914.2012.718473.

53. Rath, D.; Panda, S.; Mishra, A.; Pal, K. Particle Swarm Optimization and Machinability Aspects during Turning of Hardened D3 Steel. *J. Adv. Manuf. Syst.* **2020**, *19*, 641–662. https://doi.org/10.1142/S021968672050033X.
54. Van, A.-L.; Nguyen, T.-T.; Dang, X.-B. Optimization of Rough Self-Propelled Rotary Turning Parameters in terms of Total Energy Consumption and Surface Roughness. *Teh. Vjesn.* **2023**, *30*, 1728–1736. https://doi.org/10.17559/TV-20230202000308.
55. Hanafi, I.; Cabrera, F.M.; Dimane, F.; Manzanares, J.T. Application of particle swarm optimization for optimizing the process parameters in turning of PEEK CF30 Composites. *Procdia Technol.* **2016**, *22*, 195–202.
56. Vázquez, E.; Ciurana, J.; Rodríguez, C.A.; Thepsonthi, T.; Özel, T. Swarm intelligent selection and optimization of machining system parameters for microchannel fabrication in medical devices. *Mater. Manuf. Process.* **2011**, *26*, 403–414.
57. Englebrecht, A.P. *Computational Intelligence: An Introduction*; Wiley: West Sussex, UK, 2007.
58. Chen, H.; Heidari, A.A.; Chen, H.; Wang, M.; Pan, Z.; Gandomi, A.H. Multi-population differential evolution-assisted Harris hawks optimization: Framework and case studies. *Future Gener. Comput. Syst.* **2020**, *111*, 175–198. https://doi.org/10.1016/j.future.2020.04.008.
59. Liang, J.; Qiao, K.; Yu, K.; Ge, S.; Qu, B.; Xu, R.; Li, K. Parameters estimation of solar photovoltaic models via a self-adaptive ensemble-based differential evolution. *Sol. Energy* **2020**, *207*, 336–346. https://doi.org/10.1016/j.solener.2020.06.100.
60. Mkoko, Z.A. Ultra-High Precision Machining of Optical Aluminium (RSA-443). Ph.D. Thesis, Nelson Mandela University, Port Elizabeth, South Africa, 2019.
61. Piotrowski, A.P.; Napiorkowski, J.J.; Piotrowska, A.E. Particle Swarm Optimization or Differential Evolution—A comparison. *Eng. Appl. Artif. Intell.* **2023**, *121*, 106008. https://doi.org/10.1016/j.engappai.2023.106008.
62. Ejiofor, V.E.; Abou-El-Hossein, K. Optimization Strategy for Molecular Dynamics Simulations of Nanometric Cutting of Aluminium Alloy Using Molecular Modelling. *Mater. Sci. Forum* **2023**, *1084*, 79–84. https://doi.org/10.4028/p-068n78.
63. Kim, W.T.; Zhang, D.L.; Cantor, B. Microstructure of rapidly solidified aluminium-based immiscible alloys. *Mater. Sci. Eng. A* **1991**, *134*, 1133–1138. https://doi.org/10.1016/0921-5093(91)90940-O.